

## Yb/WO<sub>3</sub>/Yb back to back Schottky barriers designed as voltage controlled rectifiers and as microwave resonators

A. F. Qasrawi<sup>a,b,\*</sup>, Rana B. Daragme<sup>a</sup>,

<sup>a</sup>Physics Department, Arab American University, Jenin, Palestine

<sup>b</sup>Department of Electrical and Electronics Engineering, Istinye University, 34010 Istanbul, Turkey

Herein, *p* –WO<sub>3</sub> thin films coated onto ytterbium thin film substrates are used as active layers to fabricate a back to back Schottky (BBS) barriers. The Schottky contacts and the tungsten oxide active layers are grown by the thermal evaporation technique under a vacuum pressure of 10<sup>-5</sup> mbar. The films are structurally, morphologically, optically and electrically characterized. The physical nature of the grown *p* –WO<sub>3</sub> layers is amorphous comprising excess oxygen in its composition. Electrically, the BBS devices displayed a biasing dependent current rectification ratio confirming the tunneling type of Schottky barriers. The current conduction are dominated through tunneling barriers of height of ~0.80 eV. The barriers allow hole tunneling within energy barriers of widths of ~45 nm and of 300 nm under reverse and forward biasing conditions, respectively. In addition, the impedance spectroscopy measurements have shown the ability of wide tunability of the resistance and capacitance of the devices resulting in a microwave cutoff frequency exceeding 2.0 GHz. The resistive and capacitive features of the devices in addition to the microwave cutoff frequency spectra nominate the Yb/*p*-WO<sub>3</sub>/Yb BBS devices for use as microwave resonators suitable for 4G/5G technologies.

(Received January 8, 2022; Accepted April 9, 2022)

**Keywords:** Yb/WO<sub>3</sub>, Back to back Schottky, Microwave resonator, Rectifiers

### 1. Introduction

Tungsten oxide is a famous *p* –layer that finds applications in electrochemistry, photocatalysis, near-infrared shielding and phototherapy and sensing [1]. They also find applications as solar cells [2]. In a recent work, modification of WO<sub>3</sub> with niobium oxide resulted in solar cells of power efficiency of ~18% [2]. In addition, the controlled growth of WO<sub>3</sub> in nanowire forms by the chemical vapor deposition technique resulted in the production of ultra-long nanowires (60 μm). These nanowires are used as photosensors achieving responsivity of ~19 A/W at biasing voltage of 0.10 V [3]. The detectivity of these photosensors reached 1.06 × 10<sup>11</sup> Jones when exposed to laser light of 404 nm wavelength [3]. On the other hand, the excess or deficient oxygen is regarded as an interesting feature of this material. Oxygen deficiency in WO<sub>3</sub> is mentioned forcing remarkable decrease in the electrical resistivity of the films [4]. It is mentioned that vacant WO<sub>3</sub> exhibit lower resistivity values that nominates the films for electronic applications including resistive random-access memory devices [4, 5]. Another interesting practical application of WO<sub>3</sub> is the employment of this material for fabrication of Schottky barriers [6]. Pd/WO<sub>3</sub>/ZnO thin-film heterojunction-based Schottky barriers are found suitable for hydrogen sensing.

The applications of WO<sub>3</sub> active layer in many sectors of technology motivated us to design new class of WO<sub>3</sub> based Schottky barriers and find particular application for them in microwave technology. Thus, here in this work thin film of WO<sub>3</sub> coated onto Yb substrates and top contacted with Yb point contacts is fabricated and characterized by the X-ray diffraction, energy dispersive X-ray spectroscopy, optical spectrophotometry, current-voltage characteristics and impedance spectroscopy in the microwave frequency domain. Some particular applications will be suggested.

---

\* Corresponding author: atef.qasrawi@istinye.edu.tr

## 2. Experimental details

Tungsten oxide and ytterbium thin films are prepared by the thermal deposition technique under a vacuum pressure of  $10^{-5}$  mbar onto ultrasonically cleaned glass substrates. The source materials were  $\text{WO}_3$  powders and Yb grains of high purity (99.99%, Alpha Aesar). The cleaned glass and glass/Yb films were coated with  $\text{WO}_3$  (99.99%, Alpha Aesar) using appropriate masks. The films were prepared in a NORM VCM -600 vacuum evaporator equipped with Inficon STM-2 thickness monitor. Each of the stacked layers thicknesses were  $1.0 \mu\text{m}$ . The structural measurements were actualized with the help of Miniflex 600 X-ray diffraction (XRD) unit. The composition of the Yb/ $\text{WO}_3$  interfaces were carried out with the help EDAX type energy dispersive X-ray spectral analyzer. The  $p$ -type conductivity of  $\text{WO}_3$  was explored by the hot probe technique. The electrical measurements were carried out using Keithley I-V system. The capacitance and resistance spectra were recorded using Agilent 4291B 1.0M–1.8 GHz impedance analyzer.

## 3. Results and discussion

In the current study we used  $p$ - $\text{WO}_3$  as active layer for fabrication of new class of electronic devices applicable in microwave technology. The electron affinity and the work function of  $p$ - $\text{WO}_3$  are  $q\chi_{\text{WO}_3} = 3.33$  eV and  $q\phi_{\text{WO}_3} = 4.80$ - $5.30$  eV [7-8] (average value is 5.05 eV [9]), respectively. Formation of Schottky barrier requires metal work function less than  $q\phi_{\text{WO}_3}$ . For this reason  $\text{WO}_3$  is coated onto Yb ( $q\phi_{\text{Yb}} = 2.51$  eV [10]) thin film substrate and top contacted with point contacts of Yb of areas of  $2.41 \times 10^{-2} \text{ cm}^2$ . The schematics of the device are illustrated in the inset of Fig. 1 (a). The energy bands diagrams for the Yb/ $\text{WO}_3$ /Yb (YWY) which forms back to back Schottky (BBS) barriers is shown in Fig. 1 (a). Construction of the band diagram need information about the energy band gap, metal and semiconductor work functions and electron affinities. To determine the energy band gap, the optical transmittance ( $T$ ) and reflectance ( $R$ ) at normal incidence for  $\text{WO}_3$  were measured for  $\text{WO}_3$  films of thicknesses of  $d = 1.0 \mu\text{m}$  coated onto glass substrates. The absorption coefficient ( $\alpha = (1/d)\ln(T/((1 - R_{\text{glass}})(1 - R_{\text{glass}/\text{WO}_3})))$ ) spectra [11] of  $\text{WO}_3$  are displayed in Fig. 1 (b). It is clear from the figure that  $\alpha$  spectra exhibit strong absorption in the ultraviolet range of light. Tauc's equation for indirect allowed transitions ( $(\alpha E)^{\frac{1}{2}} \propto (E - E_g)$ [11]) which were found to be the most suitable formalism that linearizes the absorption coefficient data in the strong absorption range is also presented in Fig. 1 (b). As seen from the  $E$ -axis crossings of Fig. 1 (b) the energy band gap ( $E_g$ ) value is 3.05 eV. The value is consistent with literature data [12]. Since the energy band gap is 3.05 eV and the electron affinity of  $\text{WO}_3$  is 3.33 eV (Fig. 1 (a)). The valence band ( $E_v$ ) is centered at 6.38 eV below the vacuum level ( $E_{\text{vac}}$ ). As the work function of  $\text{WO}_3$  is 5.05 eV, the Fermi level ( $E_F$ ) of Yb lowers from vacuum level to reach equilibrium level with  $\text{WO}_3$ . Associated with this band bending mechanism a flat band barrier height of  $q\phi_b = q\chi_{\text{WO}_3} + E_g - q\phi_{\text{Yb}} = 3.87$  eV and a flat band built in potential  $qV_{bi} = q\phi_{\text{WO}_3} - q\phi_{\text{Yb}} = 2.54$  eV is expected [13]. Large  $V_{bi}$  values are advantageous for the electron-hole separation in the metal/semiconductor interface regions [13]. However, due to the crystalline nature, defects level, excess anions or cations in the active layers, the theoretically estimated  $q\phi_b$  and  $qV_{bi}$  may be significantly modified [13].

To reveal information about the physical nature of growth of the  $\text{WO}_3$  active layer, the layer was tested with X-ray diffraction (XRD) and energy dispersive X-ray spectroscopy (EDS) techniques. Fig. 1 (c) and (d) show the results of these tests, respectively. In accordance with Fig. 1 (c), except for the major peak of face centered cubic Yb (PDF card No: 00-002-1367) no sharp patterns were observed indicating the amorphous nature of the  $p$ - $\text{WO}_3$  as an active layer. Amorphous materials are mentioned being highly uniform and free of point defects and step edges. Such properties make them ideally suitable for heterostructures devices [14]. On the other hand, the EDS spectra (Fig. 1 (d)) indicated the formation of glass ( $\text{SiO}_2:\text{Na}_2\text{O}:\text{MgO}:\text{SiO}_2$ ), Yb and tungsten oxide. Gold appears because it was coated onto the active layer to prevent electron

contaminations. The elemental analysis revealed the formation of  $\text{WO}_{3.31}$  instead of  $\text{WO}_3$ . The  $\text{WO}_3$  active layers contained excess oxygen. Excess oxygen behaves as hole doping agent and increases the free hole concentration [15]. In practical applications the heavy doping establishes a dip in  $E_v$  and generates a peak in the conduction band ( $E_c$ ). Leading to further reduction in the barrier height [16].

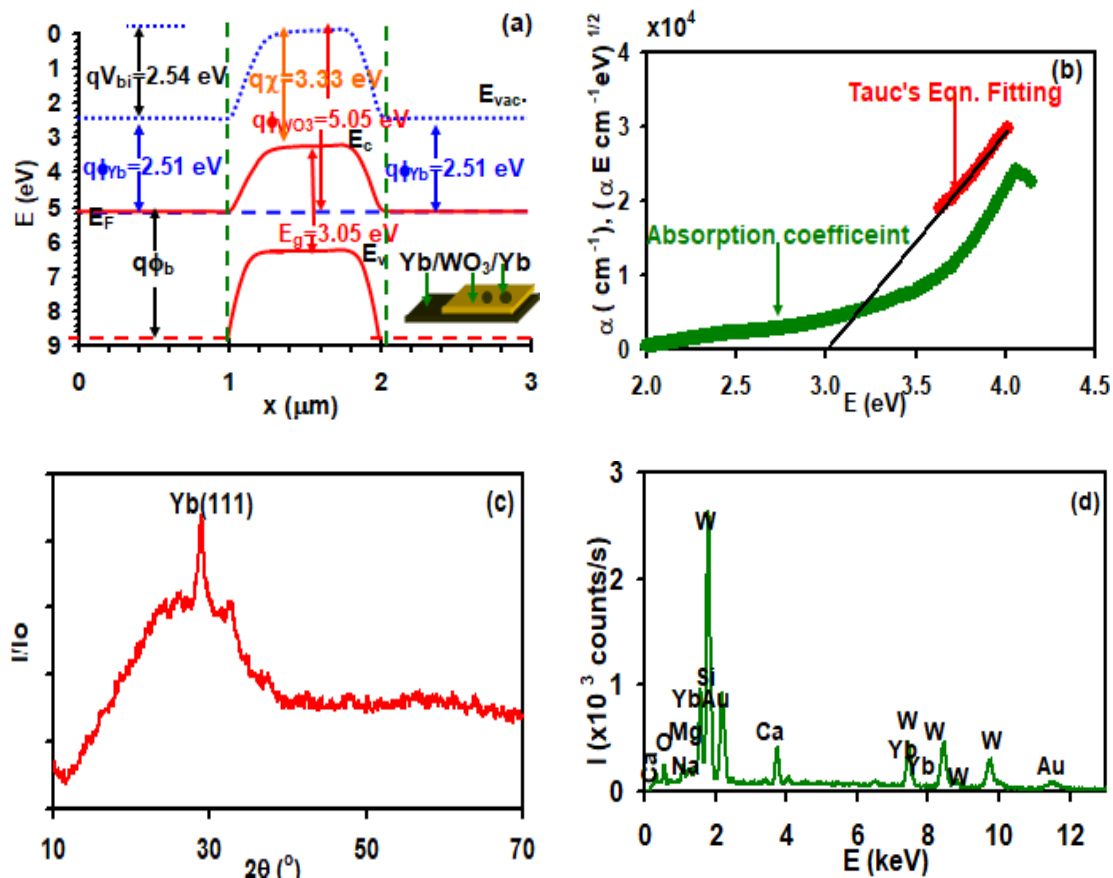


Fig. 1. (a) the energy band diagram, (b) the optical absorption and Tauc's equation fittings, (c) the X-ray diffraction patterns and (d) the energy dispersive X-ray spectra for  $\text{Yb}/\text{WO}_3/\text{Yb}$  films. The inset of (a) shows the schematics of the device.

Fig. 2 (a) illustrates the current ( $I$ )-voltage ( $V$ ) characteristics curve for the BBS devices. It is clear that the current under reverse ( $I_R$ ) biasing conditions is much higher than that under forward ( $I_F$ ) biasing conditions. The calculated current rectification ratios ( $Rec. = I_R/I_F$ ) increases with increasing biasing voltage. The higher the basing voltage, the larger the rectification ratios. This phenomenon is always observed in tunneling diodes which may have resulted from the heavy doping of holes in  $\text{WO}_3$  due to the excess oxygen as observed from the EDS measurements. The tunneling current takes the form [13, 17],

$$I_{Tun.} = AA^* T^2 V \gamma \exp\left(-\frac{e(\phi_b - n\sqrt{e\eta/(4\pi\epsilon_0\epsilon_r)}\sqrt{V}/\sqrt{w})}{kT}\right), \quad (1)$$

For Schottky Richardson type (electric field assisted thermionic emission or tunneling)  $\gamma = 0, \eta = n=1.0$  Considering the value of the Richardson constant ( $A^* = 120m_h^*$ ;  $m_h^* = 0.94m_0$  [18]), the temperature  $T = 300$  K, the dielectric constant  $\epsilon_r = 4.9$  (experimentally determined from optical data). In accordance with the linear fittings of Eqn. (1) which are shown in Fig. 2 (c), holes tunnel through barriers of height of 0.80 eV and width ( $W$ ) of 9.0 nm. Under reverse basing conditions, lowering of the barrier to 0.76 eV and slight widening to 45 nm are

reasons for the larger current values. The extremely wide tunneling barrier ( $W = 300$  nm) under forward biasing conditions accounts for the less current values compared to reverse biased diodes [13, 17].

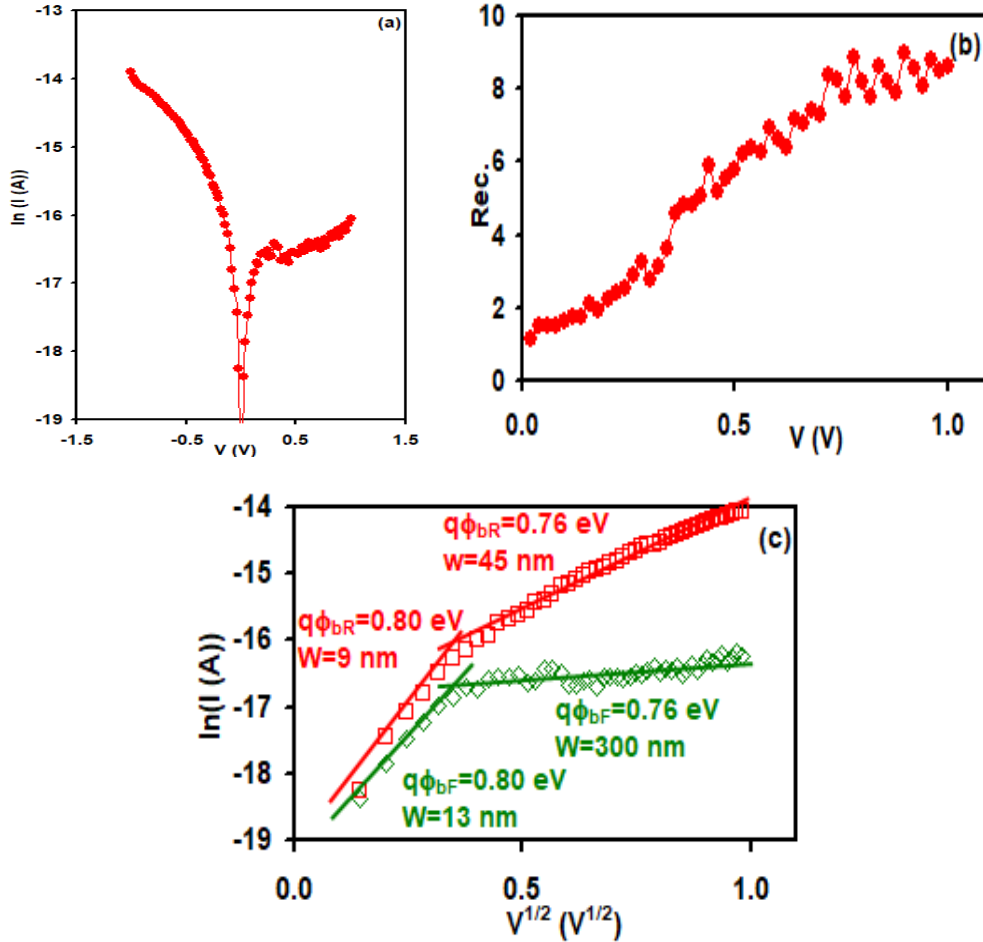


Fig. 2 (a) the  $\ln(I) - V$ , (b) rectification ratio and the  $\ln(I) - \sqrt{V}$  variation for the Yb/WO<sub>3</sub>/Yb diodes.

In addition to its workability as tunneling diodes and voltage controlled rectifiers, the frequency dependent capacitance ( $C$ ) and resistance ( $R$ ) spectra which are measured in the frequency domain of 0.01-1.80 GHz and illustrated in Fig. 3 (a) indicate frequency based tunability of these two parameters. While  $R$  values significantly decreases by more than 8 times within a short range (0.01-0.15 GHz) of frequency, the capacitance followed a slower decaying trend of variation. The overall effect can be observed from the microwave cutoff frequency ( $f_{co} = (2\pi RC)^{-1}$  [13]) spectra which are shown in Fig. 3 (b). The spectra display constant  $f_{co} = 0.33$  GHz values in the frequency domain of 0.19-0.92 GHz. It then sharply increases with increasing  $f$  values.  $f_{co}$  values larger than 2.0 GHz which is achieved at propagating signal frequency of 1.80 GHz indicate the suitability of the Yb/WO<sub>3</sub>/Yb BBS diodes as band filters for 4G/5G technologies [19].

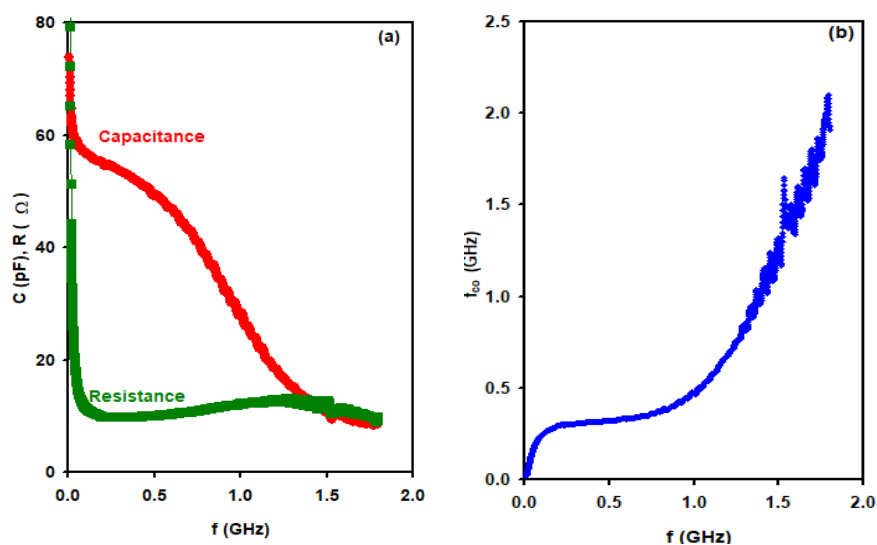


Fig. 3. (a) the resistance and capacitance spectra and (b) the microwave cutoff frequency spectra for  $\text{Yb}/\text{WO}_3/\text{Yb}$  devices.

#### 4. Conclusions

In this work we have shown the possibility of producing back to back Schottky (BBS) diodes by sandwiching  $p$ -type amorphous  $\text{WO}_3$  between two layers of ytterbium. The active layer which contained excess oxygen behaved as hole doped layer demonstrating tunneling diode characteristics. The diodes performed as biasing dependent rectifiers and as microwave cavities. The microwave cutoff frequency of the devices exceeds 2.0 GHz nominating the BBS diodes for communication technologies.

#### References

- [1] Zhang L, Wang H, Liu J, Zhang Q, Yan H. Nonstoichiometric tungsten oxide: Structure, synthesis, and applications. *J. Mater. Sci-Mater. El.* 2020;31(2):861-73; <https://doi.org/10.1007/s10854-019-02596-z>
- [2] Park HH, Kim J, Kim G, Jung H, et al. Transparent Electrodes Consisting of a Surface-Treated Buffer Layer Based on Tungsten Oxide for Semitransparent Perovskite Solar Cells and Four-Terminal Tandem Applications. *Small Methods.* 2020;4(5):2000074; <https://doi.org/10.1002/smt.202000074>
- [3] Wang H, Liu JL, Wu XX, et al. Ultra-long high quality catalyst-free  $\text{WO}_3$  nanowires for fabricating high-performance visible photodetectors. *Nanotechnol.* 2020;31(27):274003; <https://doi.org/10.1088/1361-6528/ab8327>
- [4] Romanov RI, Kozodaev MG, Lebedinskii YY, Perevalov TV, Slavich AS, Hwang CS, Markeev AM. Radical-enhanced atomic layer deposition of a tungsten oxide film with the tunable oxygen vacancy concentration. *J. Phys. Chem. C.* 2020;124(33):18156-64; <https://doi.org/10.1021/acs.jpcc.0c05446>
- [5] Balraj B, Sivakumar C, Chung PF, Bharathi M, Nagarajan SK, Ho MS. Correlation between morphology and resistive switching behaviour of  $\text{WO}_3$  nanostructures. *Mater. Lett.* 2021;308:131123; <https://doi.org/10.1016/j.matlet.2021.131123>
- [6] Liu Y, Yu J, Lai PT. Investigation of  $\text{WO}_3/\text{ZnO}$  thin-film heterojunction-based Schottky diodes for  $\text{H}_2$  gas sensing. *Int. J. Hydrogen Energ.* 2014;39(19):10313-10319; <https://doi.org/10.1016/j.ijhydene.2014.04.155>
- [7] Yuan Y, Huang J, Li G. Intermediate layers in tandem organic solar cells. *Green*, 2011. 10: 65-

80; <https://doi.org/10.1515/green.2011.009>

[8] Oh IS, Kim GM, Han SH, Oh SY. PEDOT: PSS-free organic photovoltaic cells using tungsten oxides as buffer layer on anodes. *Electron. Mater. Lett.* 2013;9(4):375-379; <https://doi.org/10.1007/s13391-013-0003-7>

[9] Halek G, Baikie ID, Teterycz H, Halek P, Suchorska-Woźniak P, Wiśniewski K. Work function analysis of gas sensitive WO<sub>3</sub> layers with Pt doping. *Sensor. Actuat. B- Chem.* 2013;187:379-385; <https://doi.org/10.1016/j.snb.2012.12.062>

[10] Khusayfan NM, Qasrawi AF, Khanfar HK. Enhancement of the performance of the Cu<sub>2</sub>Se band filters via Yb nanosandwiching. *Microw. Opt. Techn. Lett.* 2019;61(6):1449-1455; <https://doi.org/10.1002/mop.31770>

[11] Alfhaid LH, Qasrawi AF, AlGarni SE. Yb/InSe/SiO<sub>2</sub>/Au Straddling-Type Tunneling Devices Designed As Photosensors, MOS Capacitors, and Gigahertz Bandstop Filters. *IEEE T. Electron Dev.* 2021;68(3):1093-1100; <https://doi.org/10.1109/TED.2021.3049759>

[12] Ozceri E, Polat N, Balci S, Tarhan E. Room temperature emission from single defects in WO<sub>3</sub> enhanced by plasmonic nanocrystals. *Appl. Phys. Lett.* 2021;118(23):231105; <https://doi.org/10.1063/5.0048228>

[13] Sze SM, Li Y, Ng KK. *Physics of semiconductor devices.* John wiley & sons; 2021.19.

[14] Thórarinsdóttir KA, Hase T, Hjörvarsson B, Magnus F. Amorphous exchange-spring magnets with crossed perpendicular and in-plane anisotropies. *Phys. Rev. B.* 2021;103(1):014440; <https://doi.org/10.1103/PhysRevB.103.014440>

[15] Belevtsev BI, Dalakova NV, Savitsky VN, Panfilov AS, Braude IS, Bondarenko AV. Magnetoresistive study of the antiferromagnetic-weak ferromagnetic transition in single-crystal La<sub>2</sub>CuO<sub>4</sub>+ $\delta$ . *Low Tempe. Phys+.* 2004;30(5):551-557; <https://doi.org/10.1063/1.1739162>

[16] Finkman E, Shuall N, Vardi A, Le Thanh V, Schacham SE. Interlevel transitions and two-photon processes in Ge/Si quantum dot photocurrent. *J. Appl. Phys.* 2008;103(9):093114; <https://doi.org/10.1063/1.2919151>

[17] Qasrawi AF, Khanfar HK. Design and applications of Al/InSe/BN/Ag hybrid device. *IEEE Sens. J.* 2015;15(6):3603-3607; <https://doi.org/10.1109/JSEN.2015.2391202>

[18] Lin R, Wan J, Xiong Y, Wu K, Cheong WC, Zhou G, Wang D, Peng Q, Chen C, Li Y. Quantitative study of charge carrier dynamics in well-defined WO<sub>3</sub> nanowires and nanosheets: insight into the crystal facet effect in photocatalysis. *J. Am. Chem. Soc.* 2018;140(29):9078-9082; <https://doi.org/10.1021/jacs.8b05293>

[19] Chen RB, Ou XO. A hairpin DGS resonator for application to microstrip lowpass filters. *J. Electr. Eng.* 2020;71(2):110-115; <https://doi.org/10.2478/jee-2020-0016>